Swansea University
Prifysgol Abertawe

Cronfa
Setting Research Free

Cronfa - Swansea University Open Access Repository

This is an author produced version of a paper published in:
ACS Biomaterials Science & Engineering

Cronfa URL for this paper:
http://cronfa.swan.ac.uk/Record/cronfa40781

Paper:
Li, S., Zhang, J., Wang, C. & Nithiarasu, P. (2018). Atomistic Modeling of F-Actin Mechanical Responses and Determination of Mechanical Properties. *ACS Biomaterials Science & Engineering*
http://dx.doi.org/10.1021/acsbiomaterials.8b00640

This item is brought to you by Swansea University. Any person downloading material is agreeing to abide by the terms of the repository licence. Copies of full text items may be used or reproduced in any format or medium, without prior permission for personal research or study, educational or non-commercial purposes only. The copyright for any work remains with the original author unless otherwise specified. The full-text must not be sold in any format or medium without the formal permission of the copyright holder.

Permission for multiple reproductions should be obtained from the original author.

Authors are personally responsible for adhering to copyright and publisher restrictions when uploading content to the repository.

http://www.swansea.ac.uk/library/researchsupport/ris-support/

An atomistic modeling of F-actin mechanical responses and determination of mechanical properties

Si Li[1], Jin Zhang[2], Chengyuan Wang[1*], Perumal Nithiarasu[1]

1. Zienkiewicz Centre for Computational Engineering, College of Engineering, Swansea University, Bay Campus, Fabian Way, Swansea, Wales SA1 8EN, UK
2. Shenzhen Graduate School, Harbin Institute of Technology, Shenzhen 518055, China

* E-mail address of Corresponding author: chengyuan.wang@swansea.ac.uk (C. Y. Wang)

Abstract A molecular structural mechanics (MSM) model was developed for F-actins in cells, where the force constants describing the monomer interaction were achieved using molecular dynamics simulations. The MSM was then employed to predict the mechanical properties of F-actin. The obtained Young's modulus (1.92 GPa), torsional rigidity (2.36×10^{-26} Nm^2) and flexural rigidity (10.84×10^{-26} Nm^2) were found to be in good agreement with existing experimental data. Subsequently, the tension-induced bending was studied for F-actins as a result of their helical structure. Mechanical instability was also investigated for the actin filaments in filopodial protrusion by considering the reinforcing effect of the actin-binding proteins. The predicted buckling load agreed well with the experimentally obtained stall force, showing a pivotal role of the actin-binding protein in regulating the stiffness of F-actin bundles during the formation of filopodia protrusion. Herein, it is expected that the MSM model can be extended to the mechanics of more complex filamentous systems such as stress fibers and actin meshwork.

Keywords: Actin filament; Molecular dynamics simulations; Molecular mechanics; Structural mechanics model; Structural details

Introduction

Actin-filaments (F-actins) are long filamentous polymers acting as basic structural components in eukaryotic cells [1-2]. Owing to the unique molecular structures, F-actins exhibit the ability to perform a broad range of essential cellular functions in cell motility as well as in locating and transporting protein complexes in cells [3]. The filamentous structure is established via an assembly process from monomeric globular (G) actin subunits to fibrous (F) actin [4]. The twist of the actin helix determines how the subunits are positioned with respect to each other [5]. Though there exist various twists, the most frequently reported is the twin strand of beads with an angular separation between the subunits in the helix ranging from 167.14 to 166.15° [5-6].

The pivotal roles played by F-actins depend crucially on their mechanical responses/properties [7]. An in-depth understanding of F-actin mechanics is thus essential in revealing how cells fulfill their biological functions via actin cytoskeleton and offering the new design of biomimetic structure/materials by mimicking the mechanical characteristics of F-actins. The first experimental study of the mechanical properties of F-actins was conducted by Fujime [8], where the intensity of fluctuation of scattered light was measured for F-actin in solution. This was followed by a series of development in the experimental techniques used to study the thermal fluctuation of F-actins, such as optical/electron microscopy [9-11] and fluorescence light microscopy [7]. At the same time, the new techniques to measure the mechanical properties of F-actin were also reported [12-16], to name a few, electro-optic effect [12], polarized fluorescence [13] and optical tweezers [14]. In addition to the experimental work, the effort has also been devoted to theoretically characterizing the mechanics of F-actin. Some theoretical models were proposed for cytoskeleton containing F-actins [15-17] in the framework of continuum mechanics. Specially, a wormlike

chain(WLC) model was proposed for F-actin which is capable of describing the equilibrium and nonlinear dynamical properties of F-actins[18]. However, these models are unable to describe the structural details of F-actin which may exert substantial influence on the overall mechanical behavior of the protein polymer [7]. Thus, molecular dynamics (MD) technique and coarse-grained model were employed to study the monomeric features [19-23]. Compared with the dynamics simulations, the molecular structural mechanics (MSM) model is characterized by the static equilibrium feature. As a result, the MSM model is able to largely reduce the amount of calculation and improve computational efficiency, which is essential in the study of large-scale filamentous structures, such as actin bundles and MT cytoskeleton (CSK). In particular, the robustness and efficiency of the MSM model have been demonstrated in studying the mechanics of MTs [24-25]. Similar to MTs, F-actin is also a group of CSK components composed of individual filaments constructed by connecting protein monomers. The difference between MTs and F-actin lies in the overall configurations, i.e., an MT is a hollow cylinder formed by (say 13) filaments while an F-actin is a helical bundle made of two stranded protein filaments. Due to the efficient application of MSM model to MTs and the similarity between MTs and F-actin, it is of great interest to further extend the model to the mechanical behavior of F-actin.

The present study aims to achieve this goal by considering the unique features of F-actin and characterize its mechanical behavior based on the obtatined MSM model. Herein, the MSM model was first introduced and validated in measuring the elastic properties of F-actin. After this, the investigation on the unique mechanical responses was carried out for the F-actin subject to tensile or compressive axial loads. The influence of the actin-binding proteins was also examined in forming the filopodia protrusion.

Model development for F-actin

In this section, atomistic simulations were performed on the supramolecular F-actin. The MSM technique and the molecular dynamics (MD) simulation used were briefly introduced as follows.

Single F-actin model

The structure of a single F-actin was illustrated in Figure 1a where the building blocks are G-actin monomers. X-ray studies revealed that, in most cases the angular separation θ in F-actins varies from 167.14 to 166.15° [5]. Accordingly, the two typical structures of F-actin were considered in the present study, which were associated with the angular separation θ = 167.14° and 166.15°, respectively. The difference between these two typical cases thus showed the maximum influence of the variation of angle separation on the mechanical behavior of F-actin. Different diameters D of F-actin were reported in the literature. In this study, D = 7 nm was selected [26], which yields the area of cross-section around 19 nm^2 close to 18 nm^2 previously used [9] in calculating the mechanical properties of F-actin. In the MSM model (Figure 1b) of the present study, the cross-section was modeled as two tangent circles as the resultant helical geometry is a helix consisting of two strands of head-to-tail stacked monomers [3]. Moreover, the helical repeat of F-actin is denoted as 'cross-over' where the number of the subunits varies with the angular separation θ [5].

In the molecular mechanics theory, the force field is expressed in the form of steric potential energy [25]. For an F-actin structure the main types of the steric potential energy include the interaction stretching energy U_i^r, the angle bending energy U_i^φ and the dihedral angle torsional potential energy U_i^τ as shown in Figure 1c. The total potential energy U of an F-actin then reads

$$U_{bonds} = \sum_{i=1,2} \left(\sum U_i^r + \sum U_i^\varphi + \sum U_i^\tau \right) \tag{1}$$

where *i* denotes the types of interactions mentioned above (*i*=1 for the intra-strand interactions and *i*=2 for the inter-strand interactions). The corresponding expressions of interaction energy are as follows.

$$U_i^r = \frac{1}{2} k_i^r (\Delta r_i)^2,\ U_i^\varphi = \frac{1}{2} k_i^\varphi (\Delta \varphi_i)^2,\ U_i^\tau = \frac{1}{2} k_i^\tau (\Delta \Phi_i)^2, (i = 1, 2) \tag{2}$$

Here, Δr_i is the change of interaction length, $\Delta \varphi_i$ is the change of in-plane interaction angle, $\Delta \Phi_i$ is the change of out-of-plane angle, k_i^r is the force constant for interaction stretching, k_i^φ is the force constant for interaction angle bending and k_i^τ is the force constant for interaction torsion. In this study, the values of these force constants were calculated based on the MD simulations.

Herein, the MSM model (Figure 1b) was constructed to accurately describe the geometric characteristics of F-actin and model the two types of the protein interactions by elastic beams. Three main deformation patterns of the beams are stretching, bending and torsion. Thus, the total potential energy of the frame structure can be written as:

$$U_{beams} = \sum_{i=1,2} \left(\sum U_i^A + \sum U_i^M + \sum U_i^T \right) \tag{3}$$

where, U_i^A is the strain energies of a beam in tension. U_i^M is the strain energy due to bending and U_i^T is the strain energy due to torsion. Here *i* specifies the quantities of beam *i* (*i*=1 for longitudinal beams and *i*=2 for helical beams). The beam energy can be calculated by using the formulas below.

$$U_i^A = \frac{1}{2} \frac{Y_i A_i}{l_i} (\Delta l_i)^2,\ U_i^M = \frac{1}{2} \frac{Y_i I_i}{l_i} (2\Delta \alpha_i)^2,\ U_i^T = \frac{1}{2} \frac{S_i J_i}{l_i} (\Delta \beta_i)^2, (i = 1, 2) \tag{4}$$

Here, l_i is the length of the beam, Δl_i is the length change, $\Delta \alpha_i$ is the bending angle, $\Delta \beta_i$ is the torsion angle, $Y_i A_i$ is the extensional stiffness, $Y_i I_i$ is the bending stiffness and $S_i J_i$ is the torsional stiffness of the beam.

The equivalency of the F-actin structure and its MSM model can be established when the

corresponding energy in Eqs. 2 and 4 are equal, which leads to the following relationship between the force constants of the protein interactions and the stiffnesses of the space beams.

$$\frac{Y_i A_i}{l_i} = k_i^r, \ \frac{Y_i I_i}{l_i} = k_i^\varphi, \ \frac{S_i J_i}{l_i} = k_i^\tau, \ (i = 1, 2) \tag{5}$$

Thus, the structural stiffnesses can be obtained via Eq. 5 once the values of k_i^r, k_i^φ, k_i^τ were obtained for F-actin based on MD simulations. Subsequently, the stiffness matrices $\mathbf{K}$ can be constructed for the whole frame structure of F-actin and its static deformation can be calculated by using the stiffness matrix method based on the following equation

$$\mathbf{Ku} = \mathbf{F} \tag{6}$$

where $\mathbf{u}$ is the global nodal displacements and $\mathbf{F}$ is the nodal forces acting on the boundary of an F-actin. More details of the technique can be found in the Supporting Information.

Model of F-actin supported by the ABPs

A filopodia F-actin bundle consists of a number of parallel actin filaments that are bounded by the actin binding proteins (ABPs). It is thus of importance to develop a modeling technique for F-actin by considering the stiffening effect of ABPs. It was noted that different ABPs were used to construct F-actin bundles [27-32]. The present study however is focused on the F-actin bundle in filopodial protrusion. Thus ABP considered here is fascin which is prevalent in filopodia [27]. Herein, the ABPs were modeled as linear springs which are able to withstand axial tension but unable to resist compression [17, 33]. The length of ABPs was taken as 9 nm and their longitudinal repeat along an F-actin filament was 36 nm [34] (Figure 1e). Specifically, the constituent F-actins of a filopodial actin bundle are bounded to form a hexagonal lattice [35]. Accordingly, ABPs was assumed to distribute uniformly in circumferential direction as shown

in Figure 1f. The angle between adjacent ABPs is set to be 60° based on the hexagonal lattice [35]. One end of the (166.15°) F-actin was fixed and the other end was allowed to slide only along the axial direction. The external force was then applied to the two monomers of the end that is able to move. The extensional stiffness of ABPs probed by single molecule unfolding experiments ranges from 1 pN/nm to 1000 pN/nm [27]. Fitting the present model to the experimental data enables us to determine the equivalent spring constants required in the spring model for ABPs. A similar modeling technique was effectively used in studying the critical buckling force of *in vivo* MTs [36].

MD simulations on monomer interaction

As mentioned before, we obtained the force constants for the protein interactions of F-actin based on MD simulations. After that, the structural stiffnesses of the space beams required in the MSM model can be determined based on Eq. 5. The MD simulations and the experimental setup used are introduced briefly in this section. As shown above, F-actins are helical linear polymers composed of G-actin subunits [5]. Following the previously used numbering method, each subunit is labeled by an integer, *n-1*, *n*, *n+1* or *n+2* (Figure 2a) from the barbed-end side of the filament [3]. The intra-strand interaction (interaction 1) of G-actins was defined as longitudinal interaction and the inter-strand one (interaction 2) as the helical interaction. Both intra- and inter-strand interactions comprise of two different interactions, such as the interaction between two monomers at their interface and the interaction inside individual monomers. To characterize these interactions, an AFM-like approach was applied with NAMD package [37]. The atomic structure of monomeric actin labeled by PDB ID code 1J6Z [38] was considered in the development of the model. The details of the structure can be found in RSCB Protein Data Bank [39]. Herein, two different molecular systems shown in Figures 2b-e were generated, i.e., the intra-strand (*n*~*n+2*) interaction and

the inter-strand (*n*~*n+1*) interaction, each of which consists of two monomers. The filament model by Egelman et al. [5] was employed to describe the initial organization between monomers. The structural data of globular (G-) actin are used in the present MD simulations to represent those of F-actin with conformation or filamentous state different from that of G-actin [38]. Such a replacement was applied successfully to characterize F-actin in previous studies [19-20]. The characterization of the inter-strand monomer interaction (between the monomers *n* and *n*+1 (Figures 2b-c)) was performed via MD simulations where a group of C_α-atoms of the residues in monomer *n* + 1 (denoted as Pulled-G) were pulled by an external load (Figures 2b-c), while another group of C_α-atoms of the residues from monomer *n* (denoted as Fixed-G) were fixed. Similar techniques were used for the intra-strand monomer interaction (between monomers *n* and *n+2* (Figures 2d-e)). In this case, the Pulled-G and Fixed-G were chosen from monomer *n+2* and monomer *n*, respectively. Herein, the Pulled-G and Fixed-G were chosen from the residues involved in the interactions between the actin monomers in F-actin structure by following Ref. 3. In addition, more detailed study was conducted to examine the influence of different choices[3] of the groups. It was found that the force-displacement relation only changes slightly when different groups were selected. Thus, the results based on the selected Pulled-G and Fixed-G in the present work should be reliable. The CHARMM22 force field [40] was used in the simulations of actins. The entire system was solved by water molecules, neutralized with Potassium chloride [20], and then energy minimized, heated to 310K and equilibrated for 5000 ps in order to stabilize the structure [41]. Then the Pulled-G were pulled by connected springs with a preliminary assigned elastic constant k_{es}= 6.948 nN/nm. The selected value of k_{es} represents a compromise between low k_{es} values that make the MD simulations very time consuming and high k_{es} values which allow faster simulations but introduce large uncertainty in the force

values. The Langevin dynamics was specified as inactive during the steered MD simulations in order to disturb the movement of the atoms as little as possible. In the tensile and bending tests, the free end of a spring was moved at a constant rate [42]. It is noted that the force-deformation behavior of proteins (e.g., collagen triple helix) may show the strain rate-dependence in tensile test [43]. Thus, in this study we examined the influence of strain rate on the force constants. It was found that the equivalent force constant converges when the rate is under 1×10^{-4} nm/ps. Hence, in what follows the rate 5×10^{-5} nm/ps was used in the simulations. Three replicas of simulations were then performed for each interaction system. The values of material property were calculated as the average value of the material property achieved in the three simulations.

Mechanical tests based on the MSM

Based on the MSM and the obtained force constants, we performed tensile, bending and torsion tests for F-actin. The goal is to calculate the corresponding elastic properties of F-actin and examine the effect of actin structure on the properties. In measuring Young modulus, one end of the F-actin was fixed, i.e., all degree of freedom was constrained to zero, while an external force F_1 is applied to the other end which is pinned to a roller free to move in longitudinal direction (Figure 3a). The value of the Young's modulus Y can then be obtained by $Y = \frac{F_1 / A_0}{\Delta L / L_0}$, in which A_0 is the area of the cross section, L_0 is the initial length and ΔL is the elongation in the axial direction. The torsion simulation was also performed for the F-actin (Figure 3b), where cantilevered F-actin was considered and a torsional moment M was applied to the monomer of the free end. The torsional rigidity κ^T was computed as $\kappa^T = ML_0 / \gamma$ [44] where γ was the torsional angle generated by M. A cantilevered F-actin was also considered in the bending

test as shown in Figure 3c. Here the bending stiffness *(EI)* is calculated by $(EI) = F_2 L_0^3 / (3w)$ [44] where F_2 is the transverse force on and w is the resulted deflection of the free end.

MSM modeling on the F-actin mechanics

In this section, MD simulations and MSM model were employed to investigate the mechanical properties of F-actins. Efforts were also invested to explore their unique deformation behavior due to helical structure and the structural rigidity in forming filopodial protrusion.

Force constants and elastic properties

The force constants were calculated for F-actin by using the techniques demonstrated in the 3rd section of model development. The results from the AFM-like MD simulations were shown in Figure 4 describing the relation between the load on the Pulled-G and their displacement along the pulling direction. Following previous MD simulations [42], the maximum displacement 0.5nm or 1nm is considered for the tensile and bending tests of the monomer interactions. This displacement range is selected as it reflects the range of displacement of subcellular components observed experimentally in Refs. 7, 9-10. From linear fitting to the data in Figures 4a and b, the force constants of actin stretching were obtained, i.e., $k_{helical}^{stretching} = 0.88953\ nN/nm$ for helical interactions and $k_{longitudinal}^{stretching} = 3.13099\ nN/nm$ for longitudinal interactions. It is worth mentioning that the linear interaction assumption is adopted to facilitate the development of the MSM for constituent protein monomers of F-actin. Such an assumption was efficiently used previously in developing models for and understanding the experimentally observed

mechanical behavior of protein filaments [9, 25, 42, 45-47]. The assumption is necessary here as it can greatly improve the computational efficiency of the MSM and at the same time, maintain the accuracy in solving the mechanical problems with relatively small deformation. On the other hand, in future efforts should be invested to improving the MSM model by considering the non-linear monomeric interaction and enabling the use of the MSM in large deformation problems of F-actin.

In the simulation of bending, the distance between the Pulled-G and Fixed-G was obtained as 6.046 nm and 8.644 nm in the helical and the longitudinal directions, respectively. When the translational displacement of Pulled-G is 1.0 *nm* in bending, the interaction angle changes γ_{helical}=0.16559 *rad* and $\gamma_{\text{longitudinal}}$ = 0.11575 *rad* were obtained, respectively. Herein, the bending energy is calculated by $U = \frac{1}{2} k_{translational}^{bending} (\Delta l)^2$ or $U = \frac{1}{2} k_{angular}^{bending} (\gamma)^2$, where $k_{translational}^{bending}$ is the interaction constant that can be directly obtained from Figures 4c and d, Δl is the displacement of Pulled-G in pulling direction, γ is the change of interaction angle and $k_{angular}^{bending}$ is defined as the force constant for the bending. Based on information shown above we finally arrived at $k_{angular}^{bending} = k_{translational}^{bending} \frac{(\Delta l)^2}{(\gamma)^2}$ and $k_{helical}^{bending} = 2.43112\ nN/nm$ for the helical interactions and $k_{longitudinal}^{bending} = 7.26357\ nN/nm$ for longitudinal interactions. It is noticed that the torsion of G-actins is difficult to simulate with the AFM-like MD simulation method. Thus, following the empirical treatment in Ref. 45, the force constants for the torsion of the two interactions were set as $k_{helical}^{torsion} = k_{helical}^{bending} / 50$ and $k_{longitudinal}^{torsion} = k_{longitudinal}^{bending} / 50$. The force constants were summarized in Table 1, which are obtained for the interactions between two adjacent G-actins. The stiffness of a system of four G-actins was also evaluated in Ref. 48. Using the MSM technique, the equivalent stiffness of the four G-actin systems can then be estimated based on the force constants obtain for the two actin systems in the present simulations. The result 6.67 nN/nm is found to

be within the range of [4.16, 67.7 nN/nm] achieved in the previous MD simulations [48]. Also, as will be shown later, the mechanical properties of F-actin given by the MSM model based on the obtained force constants match with many existing experimental data [5, 7-14, 26, 49-69].

Based on the MSM and the achieved force constants, tensile tests were performed for F-actins. The length of the simulated F-actins ranges from 500 to 50000 nm, while their angular separation equals to 166.15° or 167.14°. The obtained Young's modulus was plotted in Figure 5a against the length. It can be seen from the figure that *Y* decreases slightly with growing length for relatively short F-actins with length smaller than 5000 nm. The length dependence however decreases with the rising length and vanishes when the length is greater than a critical value of 10000 nm. The effect of the angular separation is also observed, i.e., when the angle decreases from 167.14° to 166.15° the Young's modulus changes slightly from 1.922 GPa to 1.915 GPa. The average Youngs modulus obtained here was about 1.92 GPa, in good agreement with the values 1.8 to 2.6 GPa reported in the literature [9, 49-51].

The torsional rigidity κ^T of F-actins is also calculated for the F-actins with different angular separations. For a given *L* the 166.15° F-actins exhibits κ^T higher than that of the 167.14° F-actins. The variation of κ^T however is small (< 2.2%) leading to an average value around 2.36×10^{-26} Nm^2 right in the range of [0.2×10^{-26}, 8.5×10^{-26} Nm^2] achieved in the literature [5, 14, 52-65].

The flexural rigidity *(EI)* is an important structural property of F-actins which measures their ability to resist the bending deformation and the structural instability of F-actins. In particular, the substantial length-dependence of *(EI)* was experimentally observed for MTs [70]. Similar feature was also reported for short *in silico* MTs whose length is smaller than 400 nm [25]. It is thus of great interest to examine the unique feature of *(EI)* and calculate its value for the F-actins. To this end, the MSM was used to perform

bending tests for the cantilevered F-actins with the length ranging from 200 nm to 2000 nm. The results were shown in Figure 5c which indicated that though *(EI)* fluctuated slightly with the length change, there did not exist a clear trend for *(EI)* to change with the length *L* or the separation angle. In other words, F-actins behave like a Euler beams with nearly constant bending stiffness about 10.84×10^{-26} Nm^2. This is different from the behavior of relatively short MTs whose *(EI)* increases with rising length as a result of the inter-protofilament sliding [71]. It should also be mentioned that the reported values of *(EI)* are in the range between 1.7×10^{-26} Nm^2 and 11×10^{-26} Nm^2 [7-14, 26, 49, 66-69], which is again in good agreement with the average value 10.84×10^{-26} Nm^2 calculated in Figure 5c based on the present MSM model. Overall, the mechanical properties given by the MSM model for F-actins are in accordance with existing experimental data. This comparison between the present MSM and existing experimental data show the clear evidence of the relevance of the MSM model to the mechanics of the F-actins. Moreover, the alteration of diameter *D* (7 to 8 nm) and subunit rise *r* (2.73 to 2.75 nm) may also occur for F-actins [5, 26, 72] which would lead to the variation of F-actin properties. The investigation on this issue based on the MSM model (See details in the Supporting Information) showed that the *D*-variation results in relative changes of 25% in Young's modulus *Y*, 17% in the torsional rigidity κ^T and 4% in bending stiffness *(EI)* of F-actins, while the relative changes of *Y*, κ^T and *(EI)* due to the variation of subunit rise is less than 1%.

It is worth mentioning that the estimation method for the force constants in Table 1 is different from the experimental setup in Ref. 42 where an external force is assumed to act at the monomer center (instead of the residues involved in the interactions between monomers). Under this assumption, the force constants for interaction stretching $k_{new}^{stretching}$ can be obtained as follows.

$$\frac{1}{k_{origin}^{stretching}} = \frac{1}{2k_{monomer}^{stretching}} + \frac{1}{k_{new}^{stretching}} + \frac{1}{2k_{monomer}^{stretching}} \quad (7)$$

where $k_{origin}^{stretching}$ is the coefficient in Table 1, and $k_{monomer}^{stretching} = 4.98733\ nN/nm$ is the force constant for monomer stretching. The values of Y, κ^T and (EI) were obtained based on this method for a 5μm-long F-actin (166.15°). The obtained $\kappa^T = 2.43\times10^{-26}$ Nm^2 and $(EI) = 12.47\times10^{-26}$ Nm^2 are similar to the values shown before, whereas $Y = 4.82$ GPa achieved here is substantially greater than the 1.92 GPa obtained previously. Since the loading condition considered in the 3rd section of model development is more practical in experiments, the force constants in Tables 1 were used in the present simulations.

Tension induced bending

The presence of internal forces within the cytoskeleton was of major interest in the current research [73]. The ability to sustain tension and compression offers the cell rigidity and maintains its structural stability [74]. It is generally admitted that F-actins could undergo tension while MTs are always compressed [74]. Specifically, in the models of the actin bundles and the tensegrity model of the cytoskeleton, F-actins play an important role in resisting tensile forces [75-76]. It is interesting to see in the tensile test of F-actin (Figure 6) that for a given tensile force F_1, the stretching of F-actin is always accompanied with a transverse deflection w, which increases with the rising contour length L. In addition, for a given L the deflection at the angle of 166.15° was found to be larger than the deflection associated with the angle of 167.14°. In addition, the tension-induced transverse deflection gradually increased with the increasing tensile force applied or the rising elongation of the F-actin (Figure 6). Similar transverse deflection was also observed for F-actin when a compressive force is applied.

To capture the underlying physics of the observation, we used polynomial functions to fit the L-w

(transverse deflection) relation obtained in the MSM simulations (Figure 6). It was found that the 2nd order polynomial was the best fit to the simulation results, which is in agreement with the bending theory of beams [44] where the deflection w of beams subject to a moment M is proportional to L^2. This infers that the bending of F-actin should be a result of a bending moment generated by the tensile force applied. Indeed, more detailed study showed that due to the helical structure of F-actins, the central axis of F-actin does not coincide with the position of the resultant force on the cross section when the tensile forces are applied through the centers of the two adjacent monomers (see Figure 6). In other words, there exists a resultant eccentric force $f_{eccentric}$ which can thus generate a bending moment $M = f_{eccentric} \cdot \Delta R$ relative to the central axis of the F-actin. Here ΔR is the distance between the eccentric force and the central axis. Consequently, the observed transverse deflection can be primarily attributed to this additional moment arising from the eccentric resultant force or the helical structure of F-actin. Moreover, a higher angular separation 167.14° results in a smaller ΔR, and thus, a lower bending moment and a smaller transverse deflection. Also, with the same bending moment the deflection of F-actin naturally grows with the increasing contour length. The eccentric force found in the F-actin thus offers a possible physical explanation for the tension-induced bending and the length and angle dependency of the bending deflection observed in the MSM simulations.

Furthermore, the boundary condition is found to be an important factor that controls the tension-induced bending. As mentioned in the 4th section of model development, during the tensile test, the force was applied on the 2 monomers which were pinned on axial rollers. As illustrated on the top of Figure 7, if the monomers were fixed on rollers in the tensile test, the deflection became negligible compared to the one associated with the pinned condition. Although the actual end condition of *in vivo* filaments are

not clear [36], the actual end condition could be reasonably assumed to be an intermediate state between the fixed end and pinned end. Thus, the bending induced by the tensile force may occur for the *in vivo* F-actin and can provide a possible explanation for the curved configuration observed for most F-actins [9, 77].

Effect of binding proteins on filopodial F-actin

Filopodia are thin, actin-rich plasma-membrane protrusions that function as antennae for cells to probe their environment [78]. The protrusive bundles in filopodia consist of F-actins cross-linked by actin-binding proteins (ABPs) (Figure 8a). The growth of these F-actins generates force for protrusion of the leading edge during cell motility [79]. In the study of the filopodial protrusion, the major issues are (1) the upper limit of the force the F-actin filaments can generate and (2) the underlying physical mechanisms based on which the critical value can be determined. The critical buckling load of the actin bundles may serve as a criterion in evaluating the stall force on the actin bundle [80-81] and the maximum length of the filopodial protrusion. In the meantime, a ratcheting model [82] considering a different mechanism was also proposed to predict the maximum force on the tip of the F-actins. It was reported in Ref. 80 that these two mechanisms may coexist and one of them can be predominant depending on the monomer concentration in cytosol. In what follows, we considered the condition at which the buckling is predominant mechanism in controlling the stall force on the filopodial actin bundles. The MSM model developed for the filopodial actin bundles was used in the buckling analyses, which is able to account for the structure-buckling response relation of the F-actin bundles. As shown in Figure 8a, though the length of filopodia is only about 1 to 5 μm [83], the entire length of the protrusive actin bundle inside filopodial

could be of the order of 10 μm [80, 84-85]. Therefore, to study the buckling or stall force of protrusion, we considered F-actin filament with the length varying from 0.5 to 30 μm.

To explore the buckling behavior and obtain the critical buckling load for the filopodial actin filaments, we consider two types of the filaments found in experiments whose angular separations are 166.15° and 167.14°, respectively. Herein, the buckling deformation and the length-dependence of the critical buckling load N_{cr} were shown for the F-actins with and without ABPs in Figure 8b. As plotted in Figure 8b for a single F-actin without ABP support, N_{cr} generally decreased with rising length. Specifically, the curves associated with two angular separations nearly coincide with each other. In other words, the angular separation does not exert significant influence on the buckling of the filaments.

It was reported in Ref. 80 that the bundles of parallel F-actin such as those found in filopodia cannot automatically cooperate in a linear manner to increase the amount of force generated at the bundle tip. Only the longest one in the bundle is in contact with the barrier, which thus solely resist the axial load [80]. It can be estimated from Ref. 80 that the length of the load-bearing F-actin was about 10 μm, which, in Figure 8b, corresponds to N_{cr} about 0.035 pN of a single F-actins. This however is nearly two orders of magnitude lower than the experimentally measured stall force of the order of 1 pN [80]. Thus, the single F-actin model (the 1st section of model development) is unable to explain the large force measured on the tip of the F-actin. The possible stiffening effect of the ABPs has to be taken into consideration by coupling them with the F-actin model (the 2nd section of model development). In Figure 8b, a similar trend of N_{cr} is observed for the F-actins in the presence or absence of the ABPs. But the ABPs are found to be able to largely enhance the critical buckling load. This effect of the ABPs turns out to be more substantial for slender F-actins whose length is greater than 1 μm. For example, considering the F-actin with length 10

μm the ABPs of 500 pN/nm can raise N_{cr} from 0.035 pN to 3.750 pN by more than an order of magnitude. Another determinant of the stiffening effect is the equivalent extensional stiffness of the ABPs. As expected, Figure 8b shows that N_{cr} of the F-actin grows considerably with the increasing stiffness. The stiffening effect of ABPs is strong when their equivalent stiffness rises up to 50 pN/nm. In this process, N_{cr} rises by 1 to 2 orders of magnitude when the length greater than 10 μm was considered. In particular, for relatively long F-actin with length larger than 10 μm, N_{cr} is of the order of 1 pN when the modulus falls in the range of [50 pN/nm, 1000 pN/nm]. It is noted that organization of F-actins into different functional networks is regulated by a variety of ABPs [86], whose extensional stiffnesses range from 1 pN/nm to 1000 pN/nm [27]. However, more efforts in experimental studies still need to be made to obtain the exact value of the stiffnesses of the fascins, which are the bundlers in filopodia [86]. Thus, it is evident that the stiffnesses achieved in the present study are reasonable as they fall into the range of the stiffnesses of ABPs in the literature [27], although solid data on the stiffnesses of filopodial ABPs is still required to perform further comparison. Also, the MSM model is in agreement with the experiment in measuring the critical buckling load or a stall force of F-actin bundles [80].

To summarize, the above analyses show that the influence of ABPs results in a complex buckling deformation pattern, referred to as 'localized buckling' in Ref. 87, which is associated with a high critical buckling load relative to the buckling load of single F-actin without the ABPs (Figure 8b). The ABPs can firmly hold the neighboring F-actin filaments and largely prevent the filaments from sliding towards each other. The stabilizing effect of ABPs is very strong, which greatly enhances the structural stiffness of F-actins and accordingly, enable them to elongate to an extent required for the filopodial protrusion before reaching the stall force. In other words, the ABPs play an essential role in regulating the stiffness of F-

actin bundles. The present MSM simulations thus identify the indispensable role of the ABPs in the filopodial protrusion and cell motility [84], provide a theoretical interpretation for the experimentally achieved stall force on the F-actin and propose the physical mechanism of the filopodial protrusion [80]. Here, the present work is focused on the mechanics of individual F-actin or its bundle. However, it is noted that cytosol may exert significant effect on the mechanical behaviors of F-actin. This issue thus deserves to be examined in detail in future study.

Conclusions

In the present work, the MD simulations were performed to obtain the force constants between the monomers of F-actin. Subsequently, an MSM model was first obtained for F-actin based on the structural mechanics theory and the force constants obtained. The MSM model enjoys the highly improved efficiency and expanded the scope of the research as compared with formidable MD simulations and difficult nanoscale experiments.

Based on the MSM, the effect of the structure on the elastic modulus and structural stiffnesses was investigated for F-actin. The obtained average effective Young's modulus Y = 1.92 GPa, torsional stiffness $\kappa^T = 2.36\times10^{-26}$ Nm^2, and bending stiffness $(EI) = 10.84\times10^{-26}$ Nm^2 were found to be in good agreement with existing experimental data. The results demonstrated the reliability and robustness of the present MSM model in characterizing mechanical behavior of F-actins.

The MSM model also showed that the helical structure of F-actin leads to a resultant eccentric force and thus, a resulted bending moment on the cross section of the F-actin filament when an axial tension/compression is applied. For a given axial load the induced bending deflection of F-actin increases

substantially with the rising contour length but decreases slightly with growing rotation angle. This study provided a possible physical origin for the curved F-actin filaments experimentally observed.

Furthermore, for an F-actin bundle in the filopodial protrusion the compressive load from cell membrane can be taken by only one F-actin filament supported by the ABPs that enhance the critical buckling load by one to two orders of magnitudes. The achieved buckling load is of the order of 1 pN consistent with the experimentally measured stall force on the tip of the F-actin. The ABPs thus plays a crucial role in regulating the stiffness of F-actin bundles, facilitating the formation of the filopodial protrusion and thus, cell motility.

Herein, it is highly expected that the present MSM model can be further extended to more complex filamentous systems and thus, is able to expand the scope of research to the higher order cytoskeletal structures composed of cross-linked F-actin bundles, such as the stress fibers or actin meshwork.

Conflicts of interest

There are no conflicts to declare.

Acknowledgments

S. Li acknowledges the support from the China Scholarship Council (CSC) and College of Engineering, Swansea University.

NAMD was developed by the Theoretical and Computational Biophysics Group in the Beckman Institute for Advanced Science and Technology at the University of Illinois at Urbana-Champaign.

Supporting Information statement

The supplementary details of the MD simulation and MSM simulation are provided in Supporting Information.

References

1. Lazarides, E., Actin, alpha-actinin, and tropomyosin interaction in the structural organization of actin filaments in nonmuscle cells. *The J. Cell. Biol.* **1976,** *68* (2), 202-219. DOI: 10.1083/jcb.68.2.202.

2. Bidone, T. C.; Kim, T.; Deriu, M. A.; Morbiducci, U.; Kamm, R. D., Multiscale impact of nucleotides and cations on the conformational equilibrium, elasticity and rheology of actin filaments and crosslinked networks. *Biomech. Model. Mechan.* **2015,** *14* (5), 1143-1155. DOI: 10.1007/s10237-015-0660-6.

3. Oda, T.; Iwasa, M.; Aihara, T.; Maéda, Y.; Narita, A., The nature of the globular-to fibrous-actin transition. *Nature* **2009,** *457* (7228), 441-445. DOI: 10.1038/nature07685.

4. Wegner, A., Head to tail polymerization of actin. *J. Mol. Biol.* **1976,** *108* (1), 139-150. DOI: 10.1016/S0022-2836(76)80100-3.

5. Egelman, E.; Francis, N.; DeRosier, D., F-actin is a helix with a random variable twist. *Nature* **1982,** *298* (5870), 131. DOI: 10.1038/298131a0.

6. Bourne, G. H., *Structure and Function of Muscle*. Elsevier: 2014.

7. Isambert, H.; Venier, P.; Maggs, A. C.; Fattoum, A.; Kassab, R.; Pantaloni, D.; Carlier, M.-F., Flexibility of actin filaments derived from thermal fluctuations. Effect of bound nucleotide, phalloidin, and muscle regulatory proteins. *J. Biol. Chem.* **1995,** *270* (19), 11437-11444. DOI: 10.1074/jbc.270.19.11437.

8. Fujime, S., Quasi-elastic light scattering from solutions of macromolecules. II. Doppler broadening of light scattered from solutions of semi-flexible polymers, F-actin. *J. Phys. Soc. Jpn.* **1970,** *29* (3), 751-759. DOI: 10.1143/JPSJ.29.751.

9. Gittes, F.; Mickey, B.; Nettleton, J.; Howard, J., Flexural rigidity of microtubules and actin filaments measured from thermal fluctuations in shape. *J. Cell Biol.* **1993,** *120* (4), 923-34. DOI: 10.1083/jcb.120.4.923.

10. Nagashima, H.; Asakura, S., Dark-field light microscopic study of the flexibility of F-actin complexes. *J. Mol. Biol.* **1980,** *136* (2), 169-182. DOI: 10.1016/0022-2836(80)90311-3.

11. Takebayashi, T.; Morita, Y.; Oosawa, F., Electronmicroscopic investigation of the flexibility of F-actin. *Biochimica et Biophysica Acta (BBA)-Protein Structure* **1977,** *492* (2), 357-363. DOI: 10.1016/0005-2795(77)90086-1.

12. Yoshino, S.; Umazume, Y.; Natori, R.; Fujime, S.; Chiba, S., Optical diffraction study of muscle fibers: II. Electro-optical properties of muscle fibers. *Biophys. Chem.* **1978,** *8* (4), 317-326. DOI: 10.1016/0301-4622(78)80014-3.

13. Yanagida, T.; Oosawa, F., Polarized fluorescence from ε-ADP incorporated into F-actin in a myosin-free single fiber: Conformation of F-actin and hanges induced in it by heavy meromyosin. *J. Mol. Biol.* **1978,** *126* (3), 507-524. DOI: 10.1016/0022-2836(78)90056-6.

14. Yasuda, R.; Miyata, H.; Kinosita Jr, K., Direct measurement of the torsional rigidity of single actin filaments. *J. Mol. Biol.* **1996,** *263* (2), 227-236. DOI: 10.1006/jmbi.1996.0571.

15. Howard, J., *Mechanics of motor proteins and the cytoskeleton*. Sinauer: 2005.

16. Panyukov, S.; Rabin, Y., Thermal fluctuations of elastic filaments with spontaneous curvature and

torsion. *Phys. Rev. Lett.* **2000,** *85* (11), 2404. DOI: 10.1103/PhysRevLett.85.2404.

17. Mehrbod, M.; Mofrad, M. R., On the significance of microtubule flexural behavior in cytoskeletal mechanics. *PLoS One* **2011,** *6* (10), e25627. DOI: 10.1371/journal.pone.0025627.

18. Heussinger, C.; Bathe, M.; Frey, E., Statistical mechanics of semiflexible bundles of wormlike polymer chains. *Phys. Rev. Lett.* **2007,** *99* (4), 048101. DOI: 10.1103/PhysRevLett.99.048101.

19. Chu, J.-W.; Voth, G. A., Coarse-grained modeling of the actin filament derived from atomistic-scale simulations. *Biophys. J.* **2006,** *90* (5), 1572-1582. DOI: 10.1529/biophysj.105.073924.

20. Chu, J.-W.; Voth, G. A., Allostery of actin filaments: molecular dynamics simulations and coarse-grained analysis. *Proc. Natl. Acad. Sci. U. S. A.* **2005,** *102* (37), 13111-13116. DOI: 10.1073/pnas.0503732102.

21. Deriu, M. A.; Soncini, M.; Orsi, M.; Patel, M.; Essex, J. W.; Montevecchi, F. M.; Redaelli, A., Anisotropic elastic network modeling of entire microtubules. *Biophys. J.* **2010,** *99* (7), 2190-9. DOI: 10.1016/j.bpj.2010.06.070.

22. Havelka, D.; Deriu, M. A.; Cifra, M.; Kučera, O., Deformation pattern in vibrating microtubule: Structural mechanics study based on an atomistic approach. *Sci. Rep.* **2017,** *7* (1), 4227.

23. Deriu, M. A.; Bidone, T. C.; Mastrangelo, F.; Di Benedetto, G.; Soncini, M.; Montevecchi, F. M.; Morbiducci, U., Biomechanics of actin filaments: a computational multi-level study. *J. Biomech.* **2011,** *44* (4), 630-636.

24. Li, S.; Wang, C. Y.; Nithiarasu, P., Three-dimensional transverse vibration of microtubules. *J. Appl. Phys.* **2017,** *121* (23), 234301. DOI: 10.1063/1.4986630.

25. Zhang, J.; Wang, C. Y., Molecular structural mechanics model for the mechanical properties of

microtubules. *Biomech. Model. Mechan.* **2014,** *13* (6), 1175-84. DOI: 10.1007/s10237-014-0564-x.

26. Egelman, E. H., The structure of F-actin. *J. Muscle Res. Cell Motil.* **1985,** *6* (2), 129-151. DOI: 10.1007/BF00713056.

27. Claessens, M. M.; Bathe, M.; Frey, E.; Bausch, A. R., Actin-binding proteins sensitively mediate F-actin bundle stiffness. *Nature materials* **2006,** *5* (9), 748-753. DOI: 10.1038/nmat1718.

28. Sanger, J. W.; Sanger, J. M.; Jockusch, B. M., Differences in the stress fibers between fibroblasts and epithelial cells. *The J. Cell. Biol.* **1983,** *96* (4), 961-969. DOI: 10.1083/jcb.96.4.961.

29. Bartles, J. R., Parallel actin bundles and their multiple actin-bundling proteins. *Curr. Opin. Cell Biol.* **2000,** *12* (1), 72-78. DOI: 10.1016/S0955-0674(99)00059-9.

30. Adams, J. C., Roles of fascin in cell adhesion and motility. *Curr. Opin. Cell Biol.* **2004,** *16* (5), 590-596. DOI: 10.1016/j.ceb.2004.07.009.

31. Tilney, M. S.; Tilney, L. G.; Stephens, R. E.; Merte, C.; Drenckhahn, D.; Cotanche, D. A.; Bretscher, A., Preliminary biochemical characterization of the stereocilia and cuticular plate of hair cells of the chick cochlea. *The J. Cell. Biol.* **1989,** *109* (4), 1711-1723. DOI: 10.1083/jcb.109.4.1711.

32. Lin, C.-S.; Shen, W.; Chen, Z. P.; Tu, Y.-H.; Matsudaira, P., Identification of I-plastin, a human fimbrin isoform expressed in intestine and kidney. *Mol. Cell. Biol.* **1994,** *14* (4), 2457-2467. DOI: 10.1128/MCB.14.4.2457.

33. Bathe, M.; Heussinger, C.; Claessens, M. M.; Bausch, A. R.; Frey, E., Cytoskeletal bundle mechanics. *Biophys. J.* **2008,** *94* (8), 2955-2964. DOI: 10.1529/biophysj.107.119743.

34. Ishikawa, R.; Sakamoto, T.; Ando, T.; Higashi‐Fujime, S.; Kohama, K., Polarized actin bundles formed by human fascin‐1: their sliding and disassembly on myosin II and myosin V in vitro. *J.*

Neurochem. **2003,** *87* (3), 676-685. DOI: 10.1046/j.1471-4159.2003.02058.x.

35. Claessens, M. M. A. E.; Semmrich, C.; Ramos, L.; Bausch, A., Helical twist controls the thickness of F-actin bundles. *P. Natl. Acad. Sci.* **2008,** *105* (26), 8819-8822. DOI: 10.1073/pnas.0711149105.

36. Jin, M. Z.; Ru, C. Q., Localized buckling of a microtubule surrounded by randomly distributed cross linkers. *Phys Rev E* **2013,** *88* (1), 012701. DOI: 10.1103/PhysRevE.88.012701.

37. Phillips, J. C.; Braun, R.; Wang, W.; Gumbart, J.; Tajkhorshid, E.; Villa, E.; Chipot, C.; Skeel, R. D.; Kale, L.; Schulten, K., Scalable molecular dynamics with NAMD. *J. Comput. Chem.* **2005,** *26* (16), 1781-1802. DOI: 10.1002/jcc.20289.

38. Otterbein, L. R.; Graceffa, P.; Dominguez, R., The crystal structure of uncomplexed actin in the ADP state. *Science* **2001,** *293* (5530), 708-711. DOI: 10.1126/science.1059700.

39. Berman, H. M.; Westbrook, J.; Feng, Z.; Gilliland, G.; Bhat, T. N.; Weissig, H.; Shindyalov, I. N.; Bourne, P. E., The protein data bank. *Nucleic Acids Res.* **2000,** *28* (1), 235-242. DOI: 10.1111/j.1432-1033.1977.tb11885.x.

40. MacKerell Jr, A. D.; Bashford, D.; Bellott, M.; Dunbrack Jr, R. L.; Evanseck, J. D.; Field, M. J.; Fischer, S.; Gao, J.; Guo, H.; Ha, S., All-atom empirical potential for molecular modeling and dynamics studies of proteins. *The journal of physical chemistry B* **1998,** *102* (18), 3586-3616. DOI: 10.1021/jp973084f.

41. Berendsen, H. J.; Postma, J. v.; van Gunsteren, W. F.; DiNola, A.; Haak, J., Molecular dynamics with coupling to an external bath. *The Journal of chemical physics* **1984,** *81* (8), 3684-3690. DOI: 10.1063/1.448118.

42. Deriu, M. A.; Enemark, S.; Soncini, M.; Montevecchi, F. M.; Redaelli, A., Tubulin: from atomistic

structure to supramolecular mechanical properties. *J. Mater. Sci.* **2007,** *42* (21), 8864-8872. DOI: 10.1007/s10853-007-1784-6.

43. Tang, M.; Li, T.; Gandhi, N. S.; Burrage, K.; Gu, Y., Heterogeneous nanomechanical properties of type I collagen in longitudinal direction. *Biomech. Model. Mechan.* **2017,** *16* (3), 1023-1033. DOI: 10.1007/s10237-016-0870-6.

44. Gere, J. M.; Goodno, B. J., *Mechanics of materials*. Nelson Education: 2012.

45. Ji, X. Y.; Feng, X. Q., Coarse-grained mechanochemical model for simulating the dynamic behavior of microtubules. *Phys Rev E* **2011,** *84* (3 Pt 1), 031933. DOI: 10.1103/PhysRevE.84.031933.

46. Felgner, H.; Frank, R.; Schliwa, M., Flexural rigidity of microtubules measured with the use of optical tweezers. *J. Cell Sci.* **1996,** *109* (2), 509-516.

47. Takasone, T.; Juodkazis, S.; Kawagishi, Y.; Yamaguchi, A.; Matsuo, S.; Sakakibara, H.; Nakayama, H.; Misawa, H., Flexural rigidity of a single microtubule. *Jpn. J. Appl. Phys.* **2002,** *41* (5R), 3015. DOI: 10.1143/JJAP.41.3015.

48. Li, T.; Gu, Y.; Feng, X.-Q.; Yarlagadda, P. K.; Oloyede, A., Hierarchical multiscale model for biomechanics analysis of microfilament networks. *J. Appl. Phys.* **2013,** *113* (19), 194701. DOI: 10.1063/1.4805029.

49. Dupuis, D. E.; Guilford, W. H.; Wu, J.; Warshaw, D. M., Actin filament mechanics in the laser trap. *Journal of Muscle Research & Cell Motility* **1997,** *18* (1), 17-30. DOI: 10.1023/A:1018672631256.

50. Goldman, Y. E.; Huxley, A. F., Actin compliance: are you pulling my chain? *Biophys. J.* **1994,** *67* (6), 2131. DOI: 10.1016/S0006-3495(94)80700-3.

51. Kojima, H.; Ishijima, A.; Yanagida, T., Direct measurement of stiffness of single actin filaments with

and without tropomyosin by in vitro nanomanipulation. *P. Natl. Acad. Sci.* **1994,** *91* (26), 12962-12966. DOI: 10.1073/pnas.91.26.12962.

52. Prochniewicz, E.; Janson, N.; Thomas, D. D.; De La Cruz, E. M., Cofilin Increases the Torsional Flexibility and Dynamics of Actin Filaments. *J. Mol. Biol.* **2005,** *353* (5), 990-1000. DOI: 10.1016/j.jmb.2005.09.021.

53. Yoshimura, H.; Nishio, T.; Mihashi, K.; Kinosita, K.; Ikegami, A., Torsional motion of eosin-labeled F-actin as detected in the time-resolved anisotropy decay of the probe in the sub-millisecond time range. *J. Mol. Biol.* **1984,** *179* (3), 453-467. DOI: 10.1016/0022-2836(84)90075-5.

54. Tsuda, Y.; Yasutake, H.; Ishijima, A.; Yanagida, T., Torsional rigidity of single actin filaments and actin–actin bond breaking force under torsion measured directly by in vitro micromanipulation. *P. Natl. Acad. Sci.* **1996,** *93* (23), 12937-12942. DOI: 10.1073/pnas.93.23.12937.

55. Thomas, D. D.; Seidel, J. C.; Gergely, J., Rotational dynamics of spin-labeled F-actin in the sub-millisecond time range. *J. Mol. Biol.* **1979,** *132* (3), 257-273. DOI: 10.1016/0022-2836(79)90259-6.

56. Prochniewicz, E.; Zhang, Q.; Janmey, P. A.; Thomas, D. D., Cooperativity in F-actin: binding of gelsolin at the barbed end affects structure and dynamics of the whole filament. *J. Mol. Biol.* **1996,** *260* (5), 756-766. DOI: 10.1006/jmbi.1996.0435.

57. Prochniewicz, E.; Zhang, Q.; Howard, E. C.; Thomas, D. D., Microsecond rotational dynamics of actin: spectroscopic detection and theoretical simulation. *J. Mol. Biol.* **1996,** *255* (3), 446-457. DOI: 10.1006/jmbi.1996.0037.

58. Prochniewicz, E.; Walseth, T. F.; Thomas, D. D., Structural dynamics of actin during active interaction with myosin: different effects of weakly and strongly bound myosin heads. *Biochemistry* **2004,**

43 (33), 10642-10652. DOI: 10.1021/bi049914e.

59. Prochniewicz, E.; Thomas, D. D., Differences in structural dynamics of muscle and yeast actin accompany differences in functional interactions with myosin. *Biochemistry* **1999,** *38* (45), 14860-14867. DOI: 10.1021/bi991343g.

60. Prochniewicz, E.; Thomas, D. D., Perturbations of functional interactions with myosin induce long-range allosteric and cooperative structural changes in actin. *Biochemistry* **1997,** *36* (42), 12845-12853. DOI: 10.1021/bi971201r.

61. Ostap, E. M.; Yanagida, T.; Thomas, D., Orientational distribution of spin-labeled actin oriented by flow. *Biophys. J.* **1992,** *63* (4), 966-975. DOI: 10.1016/S0006-3495(92)81684-3.

62. Moriyama, K.; Yahara, I., Two activities of cofilin, severing and accelerating directional depolymerization of actin filaments, are affected differentially by mutations around the actin‐binding helix. *The EMBO Journal* **1999,** *18* (23), 6752-6761. DOI: 10.1093/emboj/18.23.6752.

63. Forkey, J. N.; Quinlan, M. E.; Goldman, Y. E., Measurement of single macromolecule orientation by total internal reflection fluorescence polarization microscopy. *Biophys. J.* **2005,** *89* (2), 1261-1271. DOI: 10.1529/biophysj.104.053470.

64. Egelman, E. H.; DeRosier, D. J., Image analysis shows that variations in actin crossover spacings are random, not compensatory. *Biophys. J.* **1992,** *63* (5), 1299-1305. DOI: 10.1016/S0006-3495(92)81716-2.

65. Egelman, E.; Padron, R., X-ray diffraction evidence that actin is a 100 Å filament. *Nature* **1984,** *307* (5946), 56-58. DOI: 10.1038/307056a0.

66. Oosawa, F., The flexibility of F-actin. *Biophys. Chem.* **1980,** *11* (3-4), 443-446. DOI: 10.1016/0301-

4622(80)87021-9.

67. Cherepanov, D. A.; Junge, W., Viscoelastic Dynamics of Actin Filaments Coupled to Rotary F-ATPase: Curvature as an Indicator of the Torque. *Biophys. J.* **2001,** *81* (3), 1234-1244. DOI: 10.1016/S0006-3495(01)75781-5.

68. Pänke, O.; Cherepanov, D. A.; Gumbiowski, K.; Engelbrecht, S.; Junge, W., Viscoelastic Dynamics of Actin Filaments Coupled to Rotary F-ATPase: Angular Torque Profile of the Enzyme. *Biophys. J.* **2001,** *81* (3), 1220-1233. DOI: 10.1016/S0006-3495(01)75780-3.

69. Brangwynne, C. P.; Koenderink, G. H.; Barry, E.; Dogic, Z.; MacKintosh, F. C.; Weitz, D. A., Bending dynamics of fluctuating biopolymers probed by automated high-resolution filament tracking. *Biophys. J.* **2007,** *93* (1), 346-59. DOI: 10.1529/biophysj.106.096966.

70. Pampaloni, F.; Lattanzi, G.; Jonas, A.; Surrey, T.; Frey, E.; Florin, E. L., Thermal fluctuations of grafted microtubules provide evidence of a length-dependent persistence length. *Proc. Natl. Acad. Sci. U. S. A.* **2006,** *103* (27), 10248-53. DOI: 10.1073/pnas.0603931103.

71. Wang, C. Y.; Guo, Z. G.; Wang, R. J.; Luo, Y., Role of the inter-protofilament sliding in the bending of protein microtubules. *J. Biomech.* **2016,** *49* (16), 3803-3807. DOI: 10.1016/j.jbiomech.2016.10.008.

72. Von der Ecken, J.; Müller, M.; Lehman, W.; Manstein, D. J.; Penczek, P. A.; Raunser, S., Structure of the F-actin–tropomyosin complex. *Nature* **2015,** *519* (7541), 114. DOI: 10.1038/nature14033.

73. Ingber, D.; Jamieson, J., Cells as tensegrity structures: Architectural regulation of histodifferentiationby physical forces tranduced over basement membranes. *Gene Expression during Normal and Malignent Differentiation* **1985**.

74. Baudriller, H.; Maurin, B.; Cañadas, P.; Montcourrier, P.; Parmeggiani, A.; Bettache, N., Form-

finding of complex tensegrity structures: application to cell cytoskeleton modelling. *Comptes rendus mécanique* **2006,** *334* (11), 662-668. DOI: 10.1016/j.crme.2006.08.004.

75. Lim, Y. C.; Cooling, M. T.; Long, D. S., Computational models of the primary cilium and endothelial mechanotransmission. *Biomech. Model. Mechan.* **2015,** *14* (3), 665-678. DOI: 10.1007/s10237-014-0629-x.

76. Barreto, S.; Clausen, C. H.; Perrault, C. M.; Fletcher, D. A.; Lacroix, D., A multi-structural single cell model of force-induced interactions of cytoskeletal components. *Biomaterials* **2013,** *34* (26), 6119-6126. DOI: 10.1016/j.biomaterials.2013.04.022.

77. Oosawa, F.; Fujime, S.; Ishiwata, S. i.; Mihashi, K. In *Dynamic property of F-actin and thin filament*, Cold Spring Harb. Symp. Quant. Biol., Cold Spring Harbor Laboratory Press: 1973; pp 277-285. DOI: 10.1101/SQB.1973.037.01.038.

78. Mattila, P. K.; Lappalainen, P., Filopodia: molecular architecture and cellular functions. *Nature reviews Molecular cell biology* **2008,** *9* (6), 446-454. DOI: 10.1038/nrm2406.

79. Mogilner, A.; Oster, G., Cell motility driven by actin polymerization. *Biophys. J.* **1996,** *71* (6), 3030-3045. DOI: 10.1016/S0006-3495(96)79496-1.

80. Footer, M. J.; Kerssemakers, J. W.; Theriot, J. A.; Dogterom, M., Direct measurement of force generation by actin filament polymerization using an optical trap. *P. Natl. Acad. Sci.* **2007,** *104* (7), 2181-2186. DOI: 10.1073/pnas.0607052104.

81. Dogterom, M.; Yurke, B., Measurement of the force-velocity relation for growing microtubules. *Science* **1997,** *278* (5339), 856-860. DOI: 10.1126/science.278.5339.856.

82. Peskin, C. S.; Odell, G. M.; Oster, G. F., Cellular motions and thermal fluctuations: the Brownian

ratchet. *Biophys. J.* **1993,** *65* (1), 316-324. DOI: 10.1016/S0006-3495(93)81035-X.

83. Mogilner, A.; Rubinstein, B., The physics of filopodial protrusion. *Biophys. J.* **2005,** *89* (2), 782-795. DOI: 10.1529/biophysj.104.056515.

84. Vignjevic, D.; Kojima, S.-i.; Aratyn, Y.; Danciu, O.; Svitkina, T.; Borisy, G. G., Role of fascin in filopodial protrusion. *J. Cell Biol.* **2006,** *174* (6), 863-875. DOI: 10.1083/jcb.200603013.

85. Cohan, C. S.; Welnhofer, E. A.; Zhao, L.; Matsumura, F.; Yamashiro, S., Role of the actin bundling protein fascin in growth cone morphogenesis: localization in filopodia and lamellipodia. *Cytoskeleton* **2001,** *48* (2), 109-120. DOI: 10.1002/1097-0169(200102)48:2<109::AID-CM1002>3.0.CO;2-G.

86. Winder, S. J.; Ayscough, K. R., Actin-binding proteins. *J. Cell Sci.* **2005,** *118* (4), 651-654. DOI: 10.1242/jcs.01670.

87. Brangwynne, C. P.; MacKintosh, F. C.; Kumar, S.; Geisse, N. A.; Talbot, J.; Mahadevan, L.; Parker, K. K.; Ingber, D. E.; Weitz, D. A., Microtubules can bear enhanced compressive loads in living cells because of lateral reinforcement. *J. Cell Biol.* **2006,** *173* (5), 733-741. DOI: 10.1083/jcb.200601060.

Table captions

Table 1 The force constants of interactions between monomers of F-actin

Tables

Table 1 The force constants of interactions between monomers of F-actin

Description	Constant symbol	Value
Longitudinal tensile	$k_{longitudinal}^{stretching}$ (k_1^r)	3.13 nN/nm
Longitudinal bending	$k_{longitudinal}^{bending}$ (k_1^φ)	7.26 nN·nm/rad^2
Longitudinal torsion	$k_{longitudinal}^{torsion}$ (k_1^τ)	0.145 nN·nm/rad^2
Helical tensile	$k_{helical}^{stretching}$ (k_2^r)	0.890 nN/nm
Helical bending	$k_{helical}^{bending}$ (k_2^φ)	2.43 nN·nm/rad^2
Helical torsion	$k_{helical}^{torsion}$ (k_2^τ)	0.0486 nN·nm/rad^2

Figure captions

Figure 1. (a) Structural representation of an F-actin with monomer interactions 1 and 2, (b) the MSM model developed for the F-actin with elastic beams 1 and 2 characterizing interactions 1 and 2, respectively, the deformation patterns of (c) the monomer interactions of F-actin and (d) the elastic beams 1 and 2 of the MSM model, (e) F-actin bundle in the protrusion of the leading edge in motile cells, and (f) the model of F-actin supported by ABPs in filopodia protrusive.

Figure 2. Schematics of an F-actin structure showing (a) numbering method of the monomers and the deformation patterns of the monomer interactions including (b) the interaction stretching and (c) interaction bending in the helical direction, and (d) the interaction stretching and (e) interaction bending in the longitudinal direction.

Figure 3. Experimental setup in the MSM simulations for (a) tensile, (b) torsion and (c) bending tests of a cantilevered F-actin.

Figure 4. Force-displacement relation obtained for Pulled-G in pulling direction for (a) interaction stretching along (a) the helical and (b) the longitudinal directions, and interaction bending in (c) the helical and (d) the longitudinal directions.

Figure 5. The length dependence of (a) Young's modulus Y, (b) torsional rigidity κ^T and (c) flexural rigidity (EI) calculated for F-actins with angular separation of 166.15° and 167.14°, respectively.

Figure 6. The tension induced bending of F-actin

Figure 7. Boundary condition effect on F-actin stretching

Figure 8. (a) The polymerizing actin bundle which generates force for protrusion of the leading edge in motile cells and (b) Length-dependence of the critical buckling forces Ncr obtained for the F-actins supported by ABPs with different extensional stiffness.

Figures

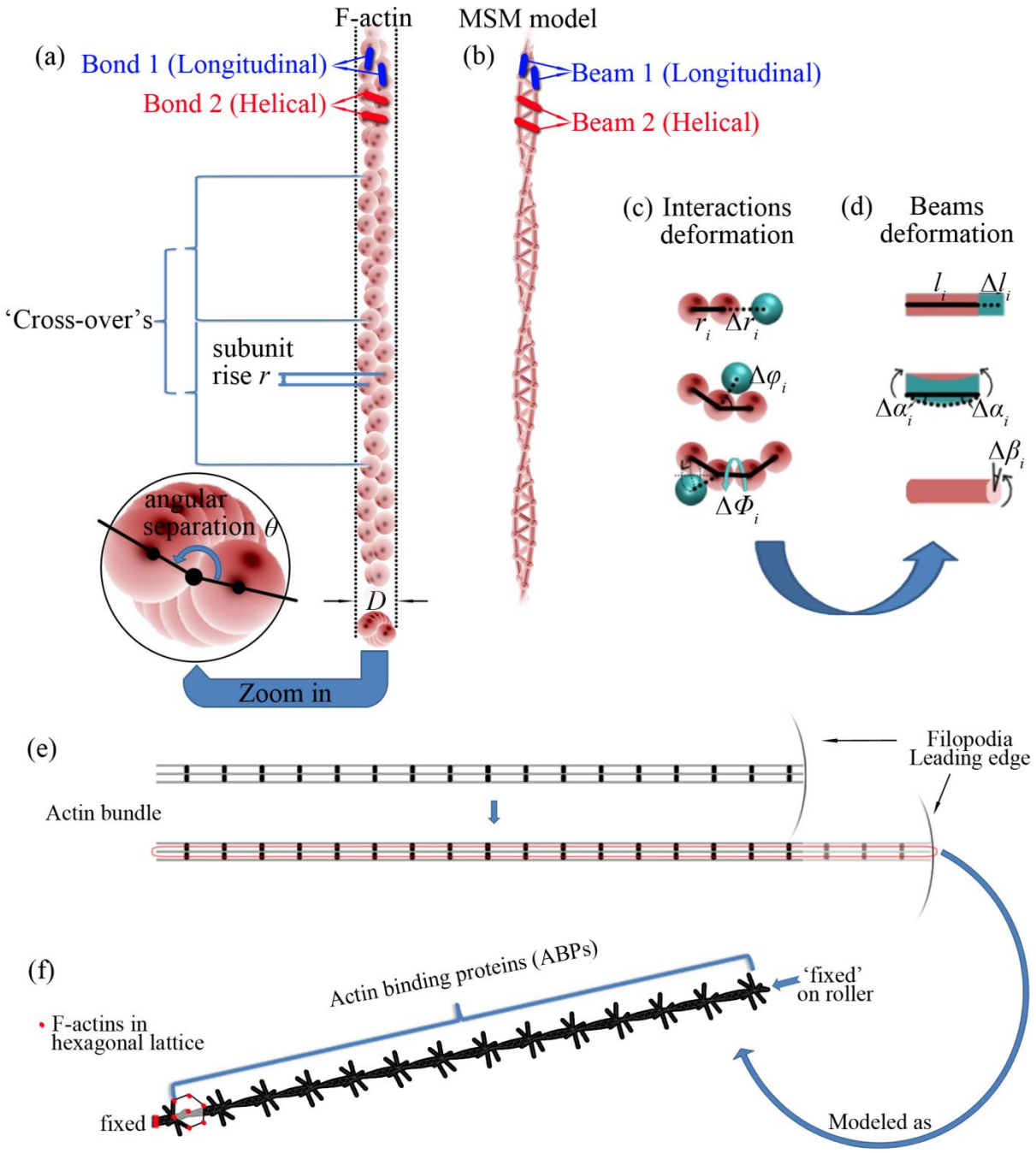

Figure 1. (a) Structural representation of an F-actin with monomer interactions 1 and 2, (b) the MSM model developed for the F-actin with elastic beams 1 and 2 characterizing interactions 1 and 2, respectively, the deformation patterns of (c) the monomer interactions of F-actin and (d) the elastic beams 1 and 2 of the MSM model, (e) F-actin bundle in the protrusion of the leading edge in motile cells, and (f) the model of F-actin supported by ABPs in filopodia protrusive.

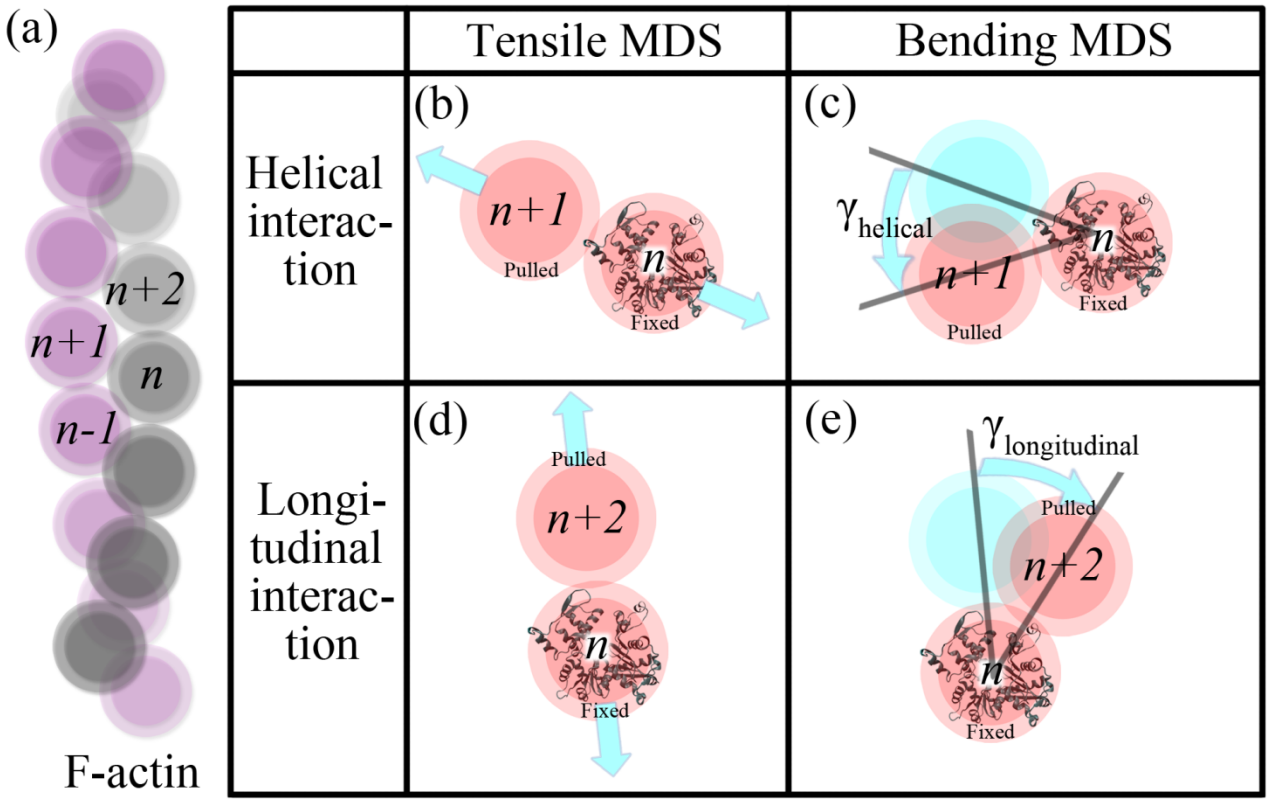

Figure 2. Schematics of an F-actin structure showing (a) numbering method of the monomers and the deformation patterns of the monomer interactions including (b) the interaction stretching and (c) interaction bending in the helical direction, and (d) the interaction stretching and (e) interaction bending in the longitudinal direction.

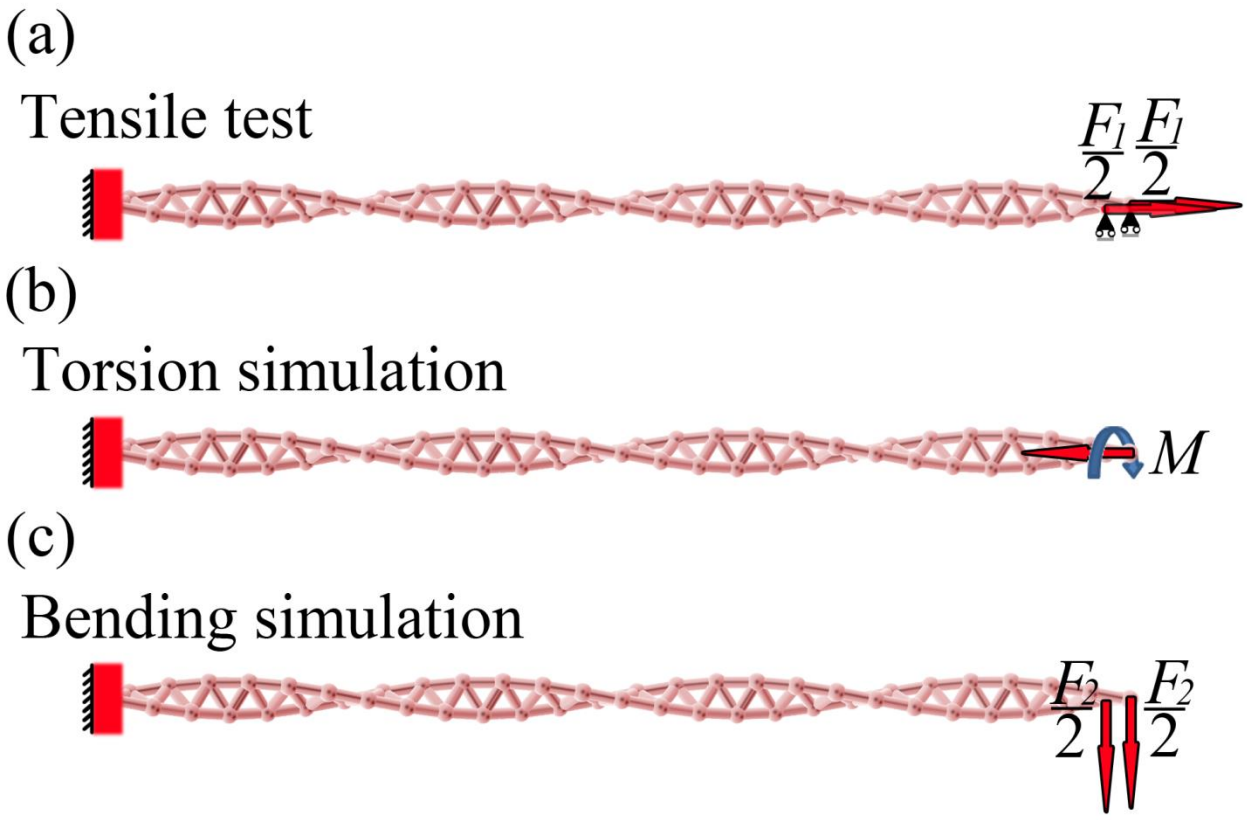

Figure 3. Experimental setup in the MSM simulations for (a) tensile, (b) torsion and (c) bending tests of a cantilevered F-actin.

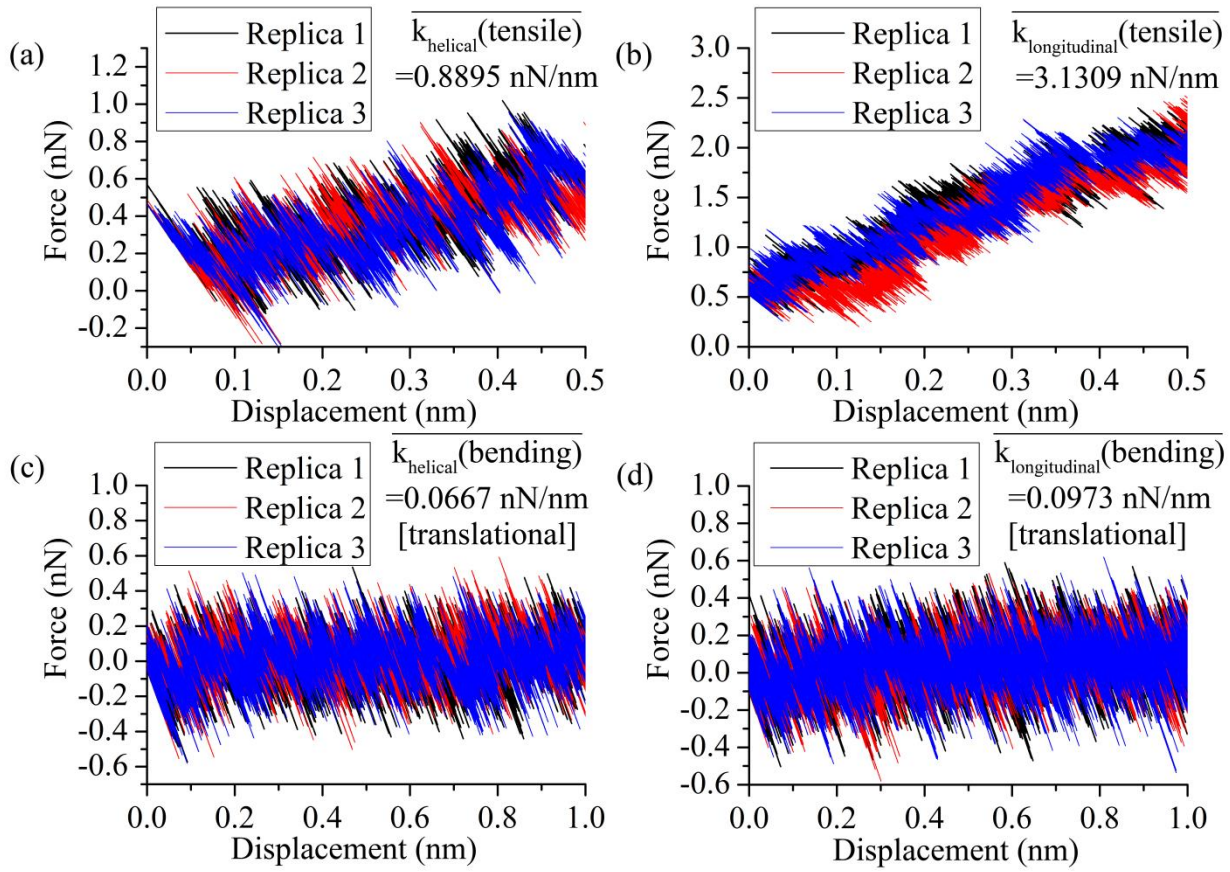

Figure 4. Force-displacement relation obtained for Pulled-G in pulling direction for interaction stretching along (a) the helical and (b) the longitudinal directions, and interaction bending in (c) the helical and (d) the longitudinal directions.

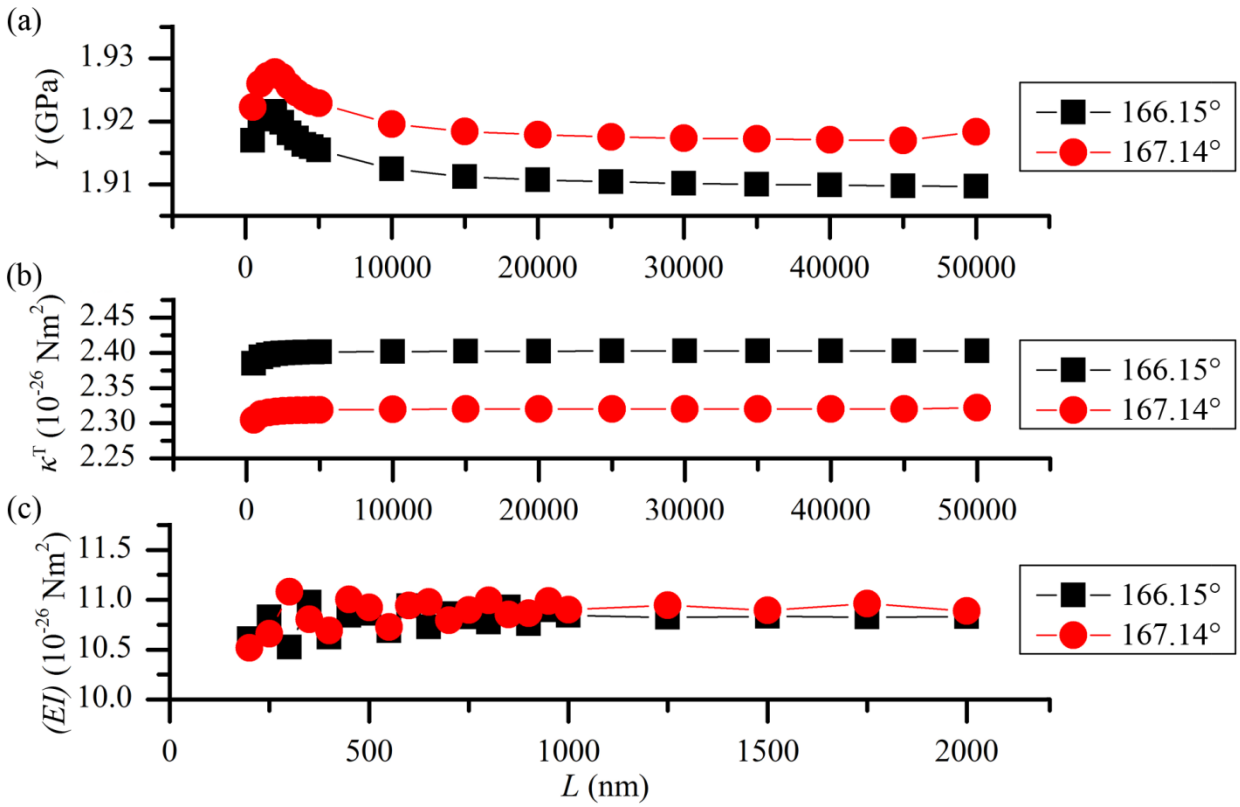

Figure 5. The length dependence of (a) Young's modulus Y, (b) torsional rigidity κ^T and (c) flexural rigidity (EI) calculated for F-actins with angular separation of 166.15° and 167.14°, respectively.

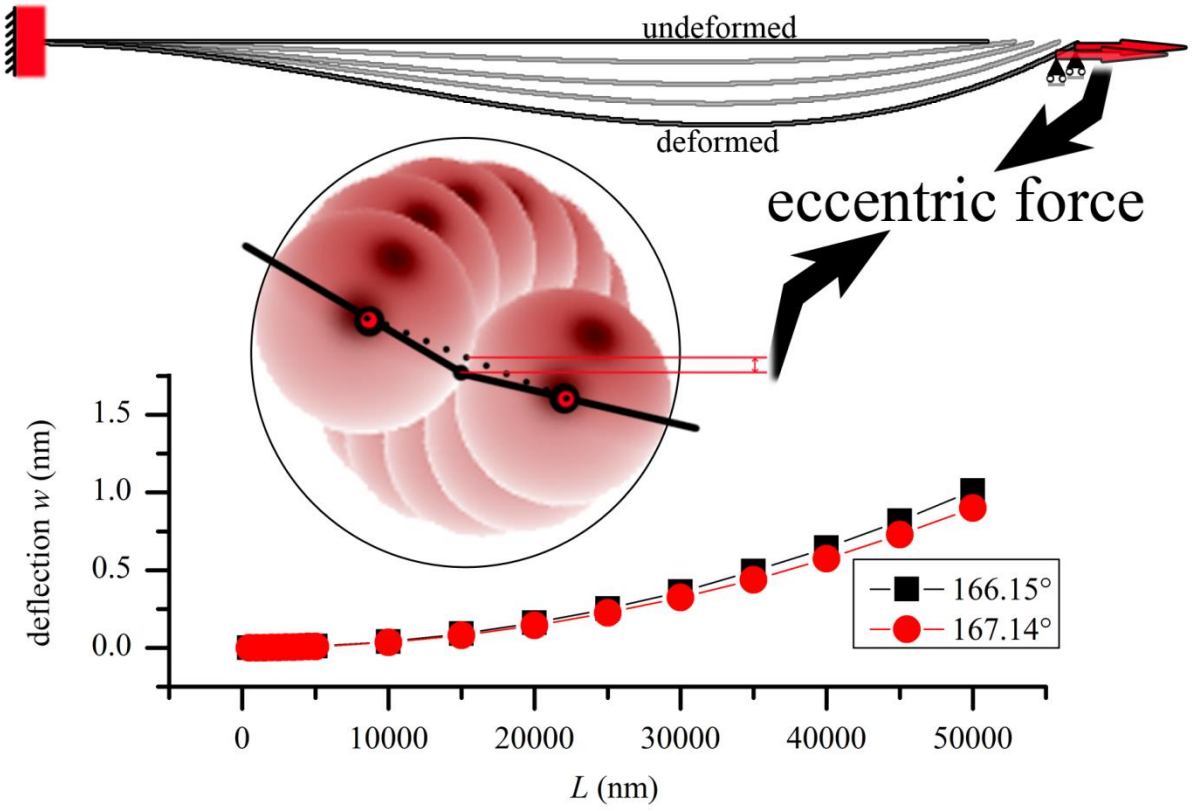

Figure 6. The tension induced bending of F-actin

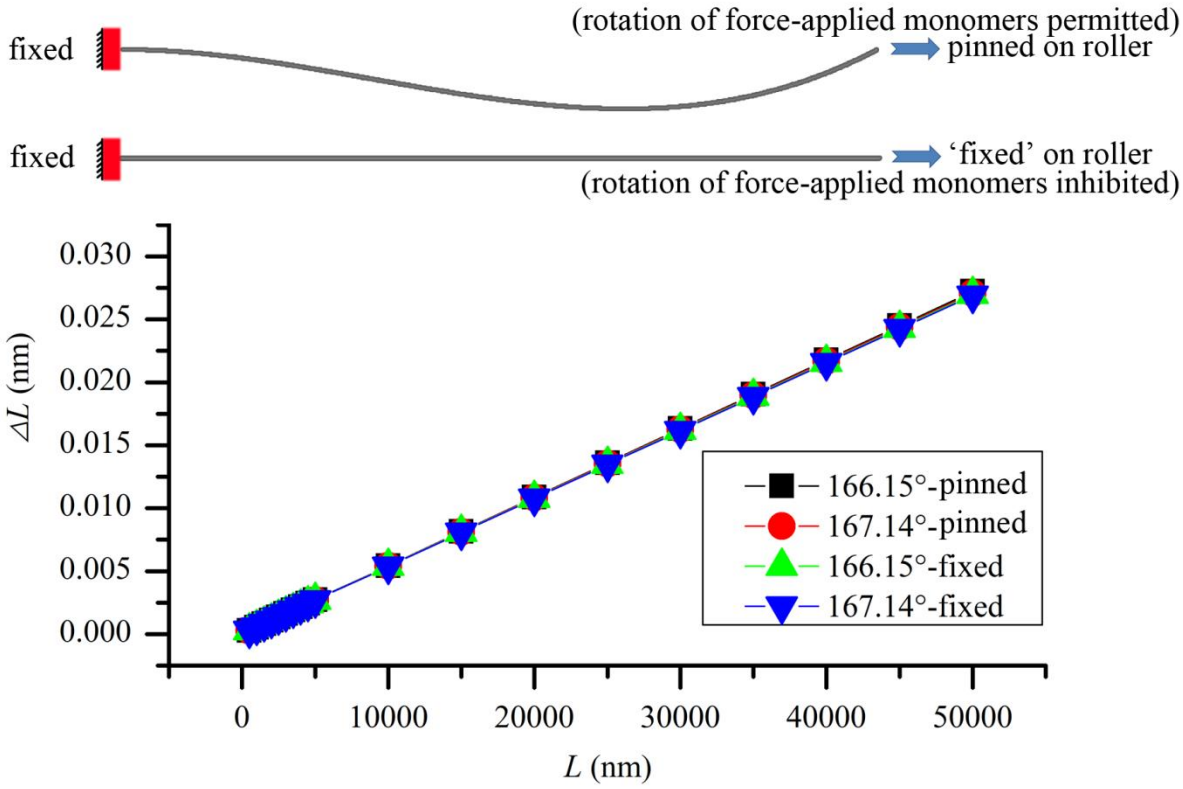

Figure 7. Boundary condition effect on F-actin stretching

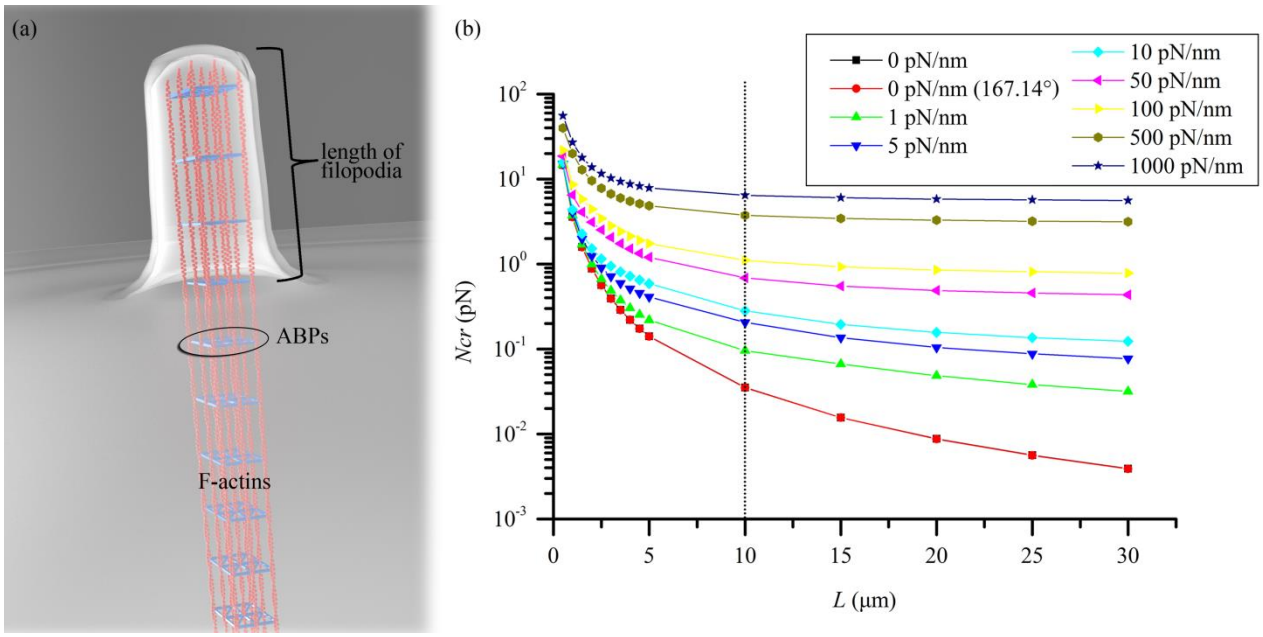

Figure 8. (a) The polymerizing actin bundle which generates force for protrusion of the leading edge in motile cells and (b) Length-dependence of the critical buckling forces *Ncr* obtained for the F-actins supported by ABPs with different extensional stiffness.

For Table of Contents Use Only

Title:

An atomistic modeling of F-actin mechanical responses and determination of mechanical properties

Authors:

Si Li, Jin Zhang, Chengyuan Wang*, Perumal Nithiarasu
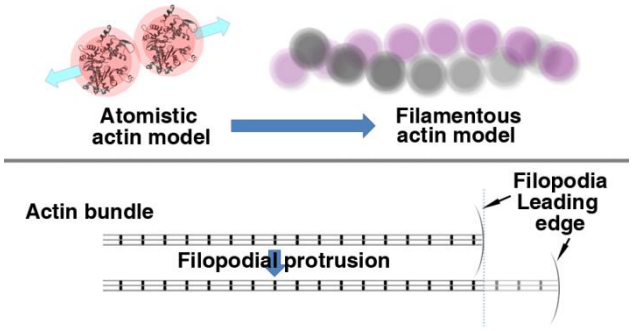
Table of Contents/Abstract Graphic: